Lamb Wave Based Experimental and Finite Element Simulation Studies for Damage Detection in an Aluminium and a Composite Plate using Geodesic Algorithm

Faeez A. Masurkar and Nitesh P. Yelve

Department of Mechanical Engineering, Fr. Conceicao Rodrigues Institute of Technology, Vashi-400703, Mumbai, India.

(Received 17 December 2014; accepted 25 February 2015)

The present research focuses on localizing structural damages in an aluminium and a woven fabric composite laminate. Finite Element (FE) and experimental simulation studies are carried out on specimens of these plates with and without damages, and the response data are collected at various sensor locations. Piezoelectric wafer (PW) transducers are used for actuation and reception of Lamb wave. The group velocity dispersion curves obtained through the experiment and simulation are compared with those obtained analytically to ensure effective actuation and sensing of Lamb wave. A Continuous Wavelet Transform (CWT) is used for receiving the arrival times of the wave reflected from the damages to the sensor locations. After acquiring arrival time data, the geodesic algorithm is employed to locate the damage in the specimens. The geodesic algorithm used is a two-step strategy initially using the Pythagorean Theorem to find the discrete geodesics in the structure, using mesh information and followed by locating the intersections of these geodesics to get the damage locations. Herein, the geodesic algorithm is shown to be effective in detecting several damages in a plate, both experimentally and through FE simulation.

1. INTRODUCTION

The process of implementing a damage detection method for civil, aerospace and mechanical engineering infrastructure is referred to as structural health monitoring (SHM). Damage is defined as a change in the material and/or geometric properties of these systems, which has an adverse effect on the system's performance. Several varieties of nondestructive tools are available for such monitoring.

Ultrasonic wave-based nondestructive evaluation (NDE) methods are widely used in investigating structures for the presence of damage, and, more recently, with a greater emphasis towards quantifying the damages; however, the conventional NDE methods, such as ultrasonic C-scan, thermography, or radiography, require the approximate location of damage to be known *a priori* and that the inspected region be directly accessible.

Further, if the structure is larger and of complex geometry, these NDE methods may not be suitable for monitoring such structures.[1] Among SHM techniques, more emphasis has been given to Lamb wave for years because of its efficiency in travelling long distances, and its propagation being affected by cracks and other structural defects.

Lamb wave-based NDE method has the potential to meet the capabilities, such as large coverage area of inspection, no need for direct access of the structure, and rapid inspection, without disassembly and adjustable frequency range for the investigation of various types of damage.[1]

A brief review about the Lamb wave-based damage detection literature is given here: Cesnik et al. gave an overview of damage prognosis, description of the basic methodology of guided wave SHM, and reviewed developments from the open literature of this multidisciplinary field.[2] Su et al. provided a comprehensive review on the Lamb wave-based damage identification approaches for composite structures.[3]

Beadle et al. studied the interaction of the first antisymmetric A_0 mode of Lamb wave in an aluminium plate with small surface notches.[4] Mofakhami et al. studied the Lamb wave propagation in an aluminium plate containing a circular hole with edge notches, both theoretically and experimentally.[5] Willberg et al. studied the use of Lamb wave for damage detection and nondestructive evaluation.[6]

Silva et al. studied a piezoelectric transducer network based system to be applied to aluminium and composite plates.[7] Kessler et al. presented the experimental and analytical survey of candidate methods for in situ damage detection of composite materials.[8] Yamada et al. studied the development of a new source location method using Lamb wave on anisotropic carbon fibre reinforced plastic plates.[9] Liu et al. studied a signal analysis method using a WT for nondestructive damage detection in the life cycle management of wind energy converters.[10]

Zabel et al. studied wavelet analysis for applying to the numerous problems within the general field of SMH.[11] Giurgiutui et al. presented the results of a systematic theoretical and experimental investigation of the fundamental aspects using PW active sensors to achieve embedded ultrasonics in thin gage beam and plate structures.[12] Finally, Gangadharan et al. proposed a geodesic-based approach using Lamb wave to locate a damage in an isotropic metallic plate.[1]

The studies presented in this literature[1] mainly focused on locating individual damage, and no FE simulation was carried out for locating them. The present work encompasses extensive experimental investigations to study the interaction of Lamb wave generated using PW transducers with damages in

metallic, as well as composite, plates. The group velocity dispersion curves obtained through experiments and FE simulations are compared with those obtained analytically. Information about the time of flight of the wave from the damage is obtained using WT, which is further used with geodesic algorithm to locate damage in the plate. Damage localisation obtained from the experiments conducted on an aluminium plate and woven fabric composite laminate are compared with those obtained through the three-dimensional FE simulation and found to be compatible.

2. FUNDAMENTALS OF LAMB WAVE

Lamb wave is a special type of ultrasonic wave that propagates in a thin plate with traction-free surfaces. Lamb wave is particularly advantageous for SHM, because it can propagate over large distances in plates and shells.[3] A Lamb wave mode can be either symmetric (S) or antisymmetric (A). In case of aluminium plates, the dispersion relations are given by[3] for symmetric modes:

$$\frac{\tan(qh)}{\tan(ph)} = -\frac{4k^2qh}{\left(k^2-q^2\right)^2}; \tag{1}$$

and for antisymmetric modes:

$$\frac{tan(qh)}{tan(ph)} = -\frac{\left(k^2-q^2\right)^2}{4k^2qh}; \tag{2}$$

where, h is the plate thickness, k is wave number, and:

$$p^2 = \frac{\omega^2}{C_{\mathrm{L}}^2} - k^2; \tag{3}$$

$$q^2 = \frac{\omega^2}{C_{\mathrm{T}}^2} - k^2; \tag{4}$$

where C_L is the longitudinal velocity of modes given by $C_L = (\lambda + 2\mu)/\rho$, C_T is transverse velocity of the modes given by $C_T = \mu/\rho$, $\lambda = Ev/((12v)(1+v))$ and $\mu = E/(2(1+v))$ are known as Lame's constants. Young's modulus is E, Poisson's ratio is v, the phase velocity is C_p, and ω is the wave circular frequency, respectively. A MATLAB© © code is written for implementing Eqs. (1) and (2) to get the dispersion curves. The roots of these equations are obtained using bisection algorithm. For group velocity (C_g) dispersion curves, the group velocity is calculated using the Eq. (5). The dispersion curves obtained are shown in Figs. 1 and 2.

$$C_g = C_p\left[1 - \frac{f}{C_p}\frac{\partial C_p}{\partial f}\right]^{-1}; \tag{5}$$

In the case of composite plates, the dispersion equations are given for symmetric case:[14]

$$\frac{\sin(kA_1h)\cos(kA_2h)}{\sin(kA_2h)\cos(kA_1h)} = \frac{A_1\left[A_2^2 - \frac{C_{11}}{C_{13}}\left(\frac{C^2}{C_{1L}^2}-1\right)\right]}{A_2\left[A_1^2 - \frac{C_{11}}{C_{13}}\left(\frac{C^2}{C_{1L}^2}-1\right)\right]} \cdot \frac{\left[\frac{C_{13}}{C_{33}}\left(\frac{C_{13}}{C_{44}}+1\right) + A_1^2 + \frac{C_{11}}{C_{44}}\left(\frac{C^2}{C_{1L}^2}-1\right)\right]}{\left[\frac{C_{13}}{C_{33}}\left(\frac{C_{13}}{C_{44}}+1\right) + A_2^2 + \frac{C_{11}}{C_{44}}\left(\frac{C^2}{C_{1L}^2}-1\right)\right]}; \tag{6}$$

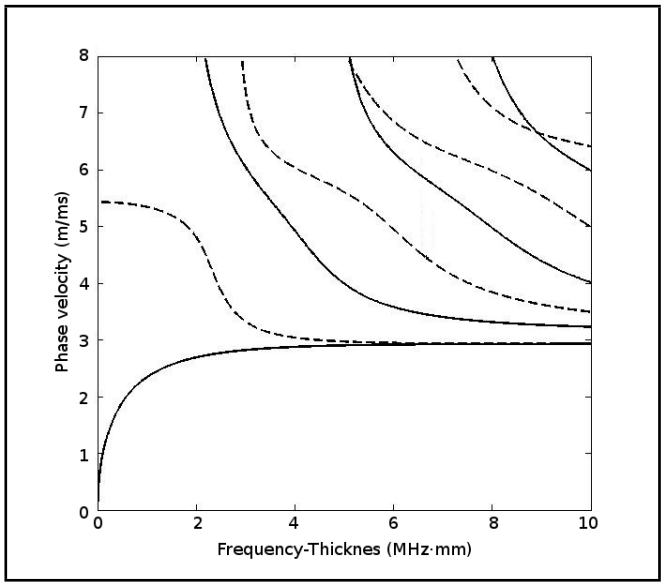

Figure 1. Phase velocity dispersion curve for an aluminium plate. Continuous lines show A modes and dotted lines show S modes.

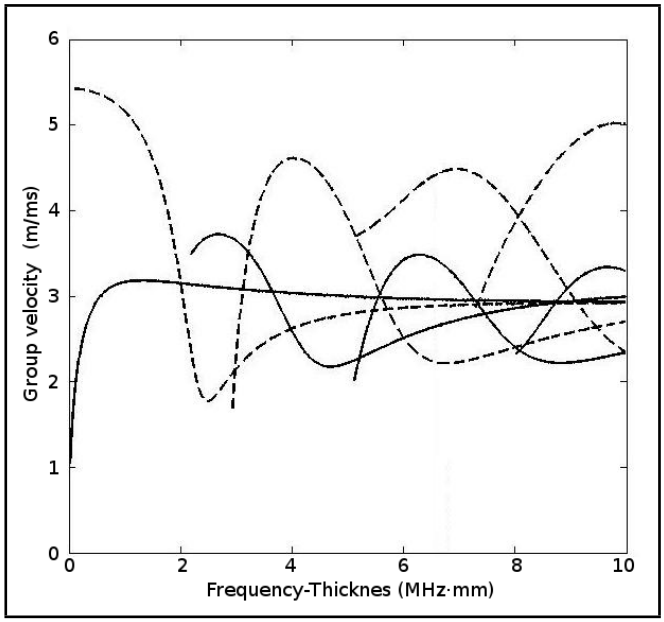

Figure 2. Group velocity dispersion curve for an aluminium plate. Continuous lines show A modes and dotted lines show S modes.

and for antisymmetric case:

$$\frac{\sin(kA_2h)\cos(kA_1h)}{\sin(kA_1h)\cos(kA_2h)} = \frac{A_1\left[A_2^2 - \frac{C_{11}}{C_{13}}\left(\frac{C^2}{C_{1L}^2}-1\right)\right]}{A_2\left[A_1^2 - \frac{C_{11}}{C_{13}}\left(\frac{C^2}{C_{1L}^2}-1\right)\right]} \frac{\left[\frac{C_{13}}{C_{33}}\left(\frac{C_{13}}{C_{44}}+1\right) + A_1^2 + \frac{C_{11}}{C_{44}}\left(\frac{C^2}{C_{1L}^2}-1\right)\right]}{\left[\frac{C_{13}}{C_{33}}\left(\frac{C_{13}}{C_{44}}+1\right) + A_2^2 + \frac{C_{11}}{C_{44}}\left(\frac{C^2}{C_{1L}^2}-1\right)\right]}; \tag{7}$$

where: $A_1 = \sqrt{\frac{-A+\sqrt{A^2-4B}}{2}}$; $A_2 = \sqrt{\frac{-A-\sqrt{A^2-4B}}{2}}$; $A = \frac{C^2}{C_{3L}^2} + \frac{C^2}{C_{3T}^2} - \frac{(C_{11}C_{33}-C_{13}^2-2C_{13}C_{44})}{C_{33}C_{44}}$ $K = \frac{\omega}{C_p}$; $C_{1\mathrm{L}}^2 = \frac{C_{11}}{\rho}$; $C_{3L}^2 = \frac{C_{33}}{\rho}$; $C_{3T}^2 = \frac{C_{44}}{\rho}$; $C_{11} = \frac{E_1(1-v_{32}v_{23})}{(1+v_{12})(1-v_{12}-2v_{32}v_{23})}$; $C_{12} = \frac{E_2(v_{12}+v_{32}v_{23})}{(1+v_{12})(1-v_{12}-2v_{32}v_{23})}$; $C_{33} = \frac{E_3(1-v_{12})}{(1-v_{12}-2v_{32}v_{23})}$; $C_{13} = \frac{v_{23}E_3}{(1-v_{12}-2v_{32}v_{23})}$; $C_{55} = G_{13}$.

A MATLAB© code is written for implementing Eqs. (6)

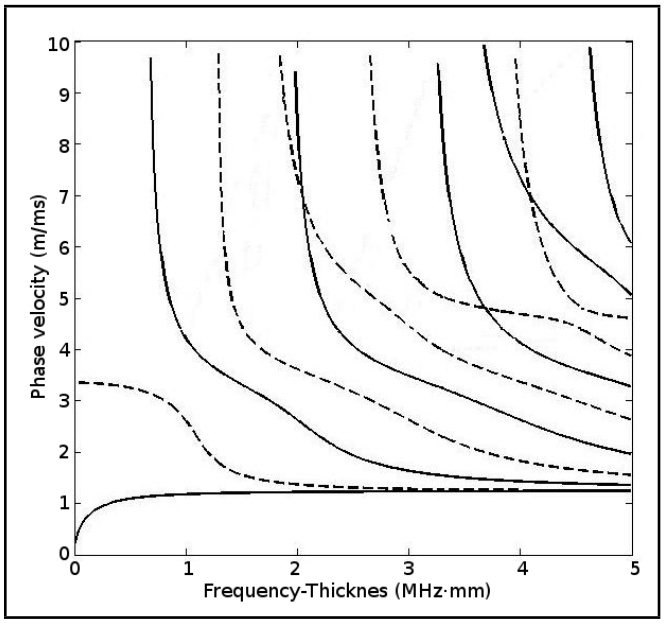

Figure 3. Phase velocity dispersion curve for a composite plate. Continuous lines show A modes and dotted lines show S modes.

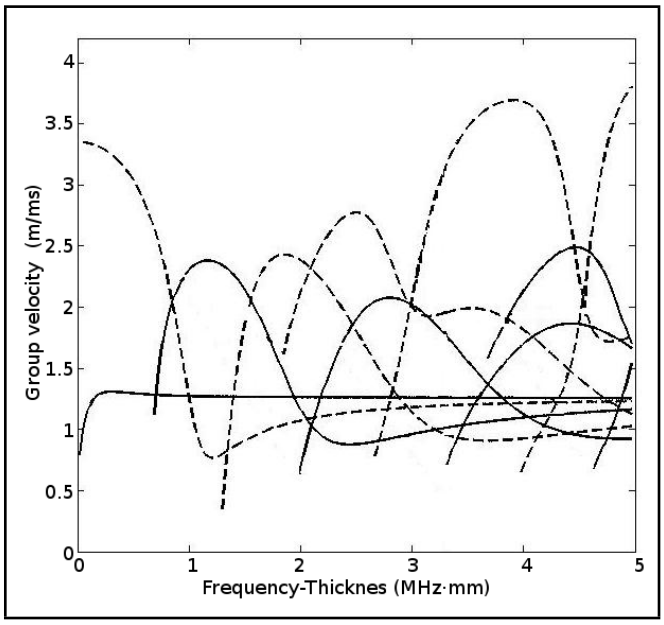

Figure 4. Group velocity dispersion curve for a composite plate. Continuous lines show A modes and dotted lines show S modes

and (7) to acquire the dispersion curves, which are shown in Figs. 3 and 4.

The dispersion curves for aluminium and composite plates demonstrate that at low frequency- thickness product, only two fundamental modes, S_0 and A_0, can propagate. With an increase in frequency-thickness product, more modes are possible and the interpretation of signals becomes more complex. Furthermore, all of the modes are dispersive, the shape of pulse signals change with the propagation time and distance, making the measurement of their arrival times difficult. The multiple-mode and dispersive characteristics of Lamb waves complicate the signal interpretations for damage identification. To avoid complications, selective generation and detection of a single mode within a frequency range to minimize the dispersion effect should be adopted.

In general, fundamental A_0 and S_0 mode are commonly

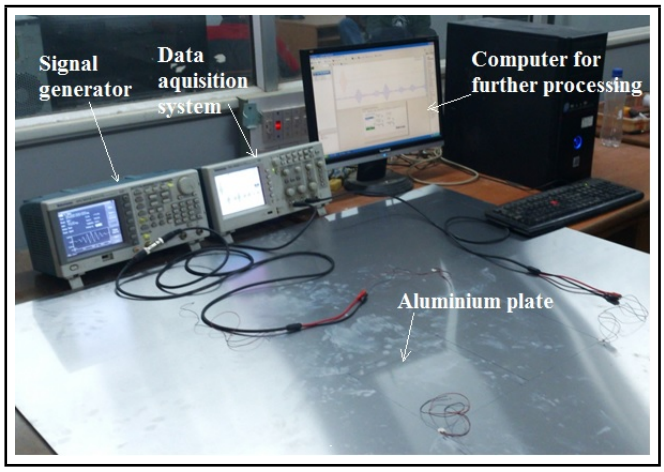

Figure 5. Experimental set-up showing signal generator and data acquisition system.

used for damage detection. The S_0 modefaster and has much lower attenuation than A_0 mode, allowing it to propagate longer distance. That said, the A_0 mode is more sensitive to small damages because of its shorter wavelength. Therefore, in the present study, the interaction between the A_0 mode and the damages is analysed.

3. EXPERIMENTAL STUDY

The experimental setup consists of a Tektronix AFG 3021B signal generator and a Tektronix TDS 1002B digital storage oscilloscope, as shown in Fig. 5. The signal generator is used to produce a tone burst signal in the form of a sine wave modulated by Gaussian window function. The Tektronix TDS 1002B digital storage oscilloscope is used for data acquisition of the response signals. The digital data are transferred to a computer for further offline processing.

The plate specimens considered here are in the form of a 1 mm thick sheet of Al-5052 aluminium alloy ($E = 70.30$ Gpa, $v = 0.33$, $\rho = 2680$ kg/m^3) and a 2 mm thick woven fabric composite laminate ($E_1 = E_2 = 24$ Gpa, $E_3 = 16$ Gpa, $G_{12} = G_{23} = G_{13} = 3$ Gpa, $\rho = 1850$ kg/m^3), where E is the modulus of elasticity, v is the Poisson ratio, ρ is the density, and G is the modulus of rigidity.

The PW transducers (material type SP-5H) of 10 mm diameter and 0.5 mm thickness are used for actuation and sensing of Lamb wave. These are bonded onto the plate using a commercially available epoxy based adhesive. The PW circular patches S_1, S_2, S_3, S_4 are bonded at locations (10 mm, 10 mm), (410 mm, 10 mm), (410 mm, 410 mm), and (10 mm, 410 mm) respectively on the plate having plan form dimensions 420 mm $\times$ 420 mm, as shown schematically in Fig. 6.

The experiments are carried out for healthy state for frequencies ranging from 50 kHz to 600 kHz in case of aluminium plate and from 85 kHz to 175 kHz in case of composite plate, and group velocities are then calculated. Excitation tone burst used is 8.5 cycle sine wave windowed by Gaussian function. For 8.5 cycles, the Lamb wave modes are seen to be well-separated, the frequency bandwidth is lessened, and the half cycle in the tone burst brings the peak amplitude to the centre which helps in calculating group velocity.

The tone burst at 8.5 cycles and 10 volt from peak to peak, supplied to PW actuator is found to possess sufficient en-

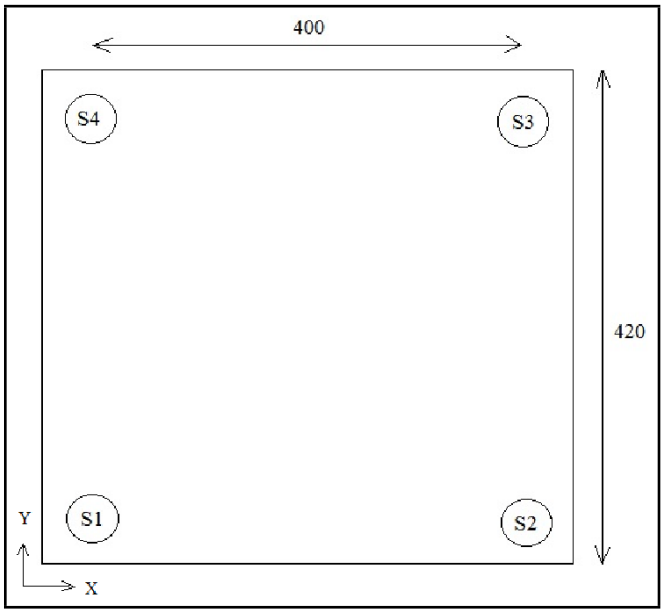

Figure 6. Plan of healthy aluminium and composite plates. All the dimensions are in millimetres.

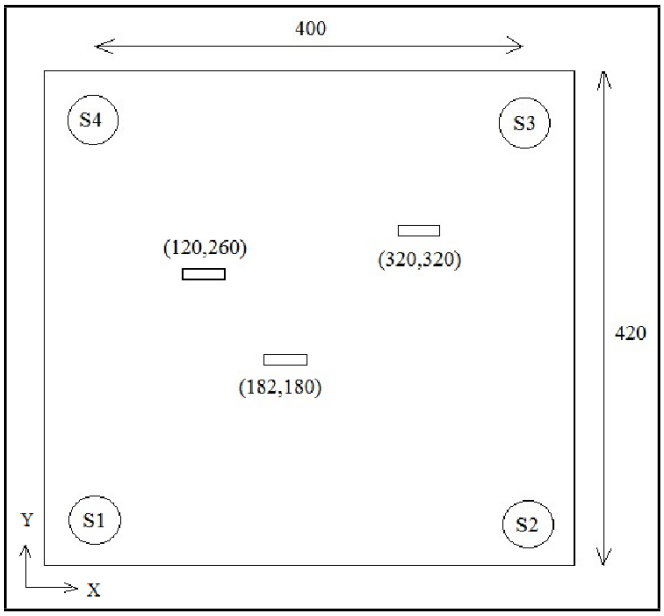

Figure 7. Plan of damaged aluminium and composite plates. All the dimensions and the cordinates of the damages are in millimetres.

ergy required for exciting the range of frequencies mentioned above. The received Lamb wave signals at the PW sensor are shown by the oscilloscope and are sent to computer for further offline signal processing.

Experimentally-obtained group velocities are compared with those obtained analytically and are found to be compatible, as shown in Figs. 8 and 9. These results demonstrate that there is effective actuation and sensing of Lamb wave, in both metallic, as well as composite plates.

Excitation frequency selection should result in quality data for the prediction of damage location and is discussed in the following subsection.

3.1. Selection of Excitation Frequency

The excitation frequency of the tone burst signal should be low enough, where only A_0 and S_0 mode can propagate. As

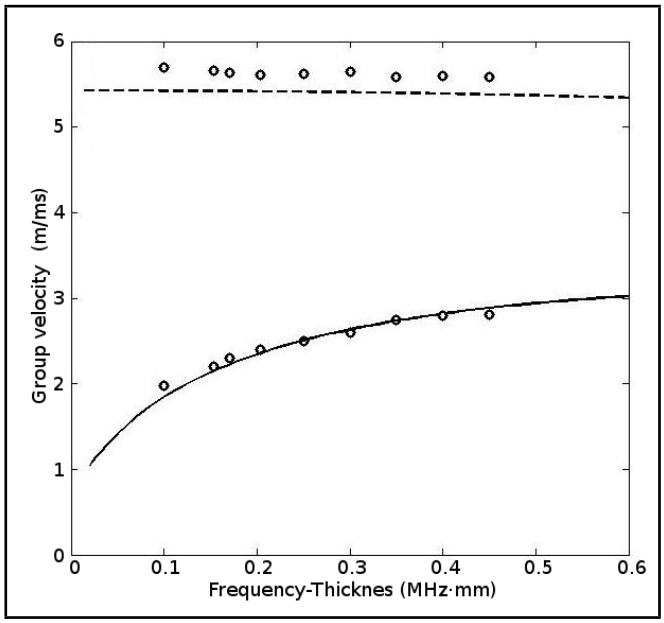

Figure 8. Comparison of analytical and experimental dispersion curves for a aluminium plate. Continuous line shows A_0 mode. The dotted line shows S_0 mode, and o shows experimental results

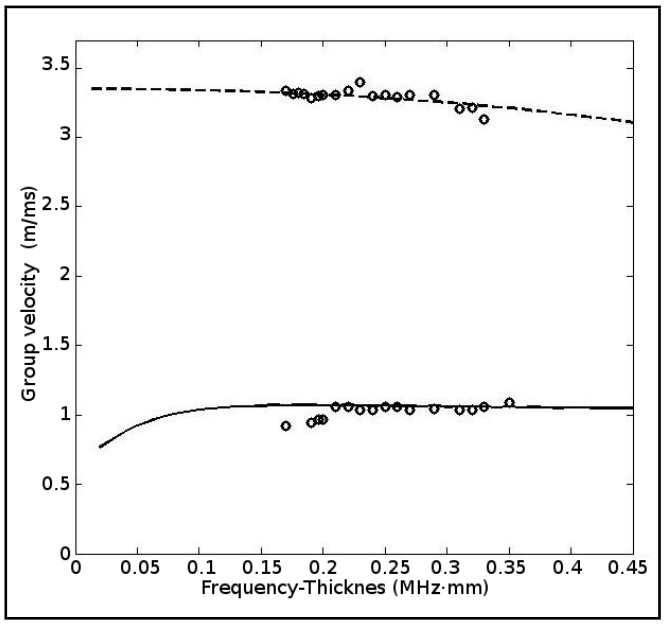

Figure 9. Comparison of analytical and experimental dispersion curves for a composite plate. Continuous line shows A_0 mode. The dotted line shows S_0 mode, and ○ shows experimental results

suggested by Giurgiutiu,[12] damage detection should be carried out at the centre frequency where the peak wave amplitude ratio between the S_0 mode and the A_0 mode is maximum.

This center frequency is referred to as the 'sweet spot'. The study by Giurgiutiu,[12] showed that when the diameter of PZT actuator is equal to odd integer multiples of half wavelength of the particular Lamb mode, strong voltage response for the corresponding Lamb mode will be produced; however, when the diameter of PZT actuator is equal to even integer multiples of half wavelength of Lamb modes, very weak voltage response will be generated.

At 204 kHz, the wavelength for A_0 mode is 6.545 mm and for S_0 mode is 27.51 mm, as can be seen from the Fig. 10, and therefore, S_0 mode can be dominantly generated. At this

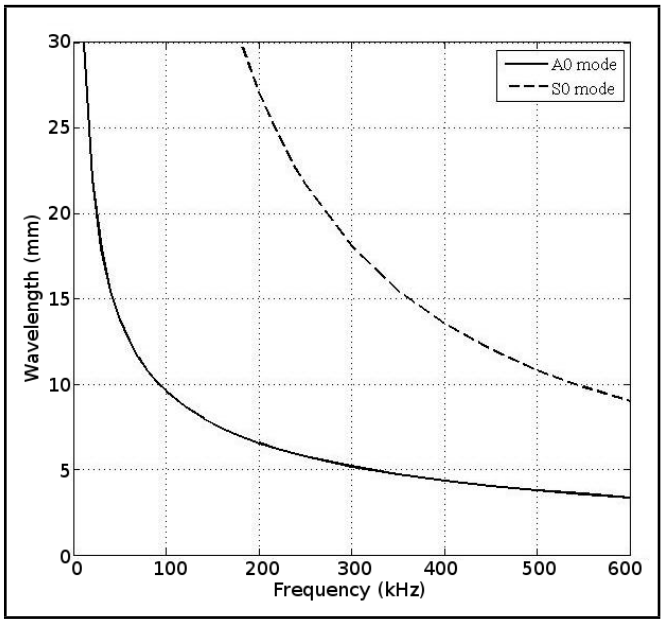

Figure 10. Wavelength dispersion for aluminium plate.

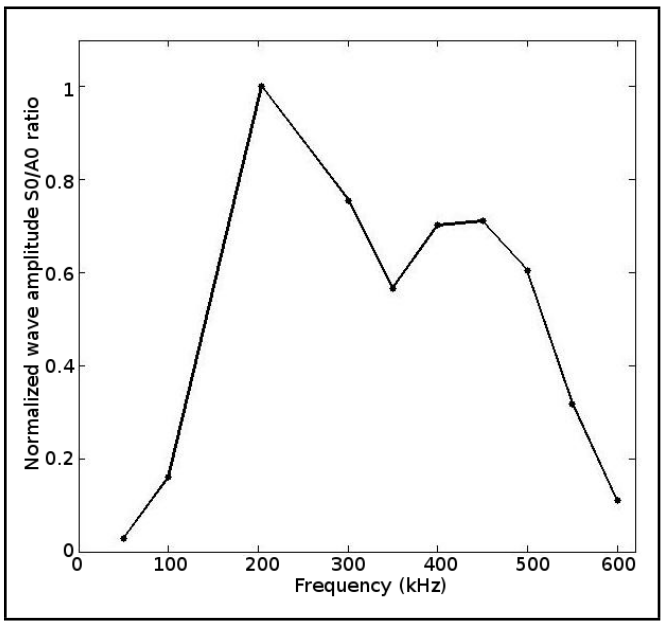

Figure 11. Experimental dispersion of S_0/A_0 ratio for aluminium plate.

frequency, maximum amplitude ratio will be obtained. The expected sweet spot' frequencies are identified to be 204 kHz for aluminium plate and 85 kHz for the composite plate, illustrated in Figs. 11 and 12.

Moreover, experiments are performed on healthy and damaged plates, shown in Figs 6 and 7 respectively, with different pairing configurations of actuators and sensors. The damages are created on the same plate used for obtaining healthy signals. Each time, one sensor acts as an actuator while the remaining three act as sensors and give 12 responses for healthy and damaged state each. Three- dimensional (3-D) FE simulations are also carried out to get Lamb wave responses, which is discussed in following section.

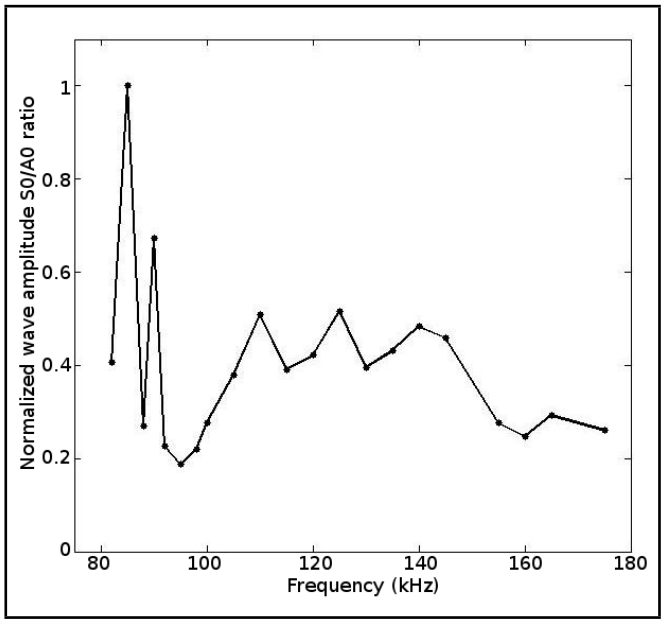

Figure 12. Experimental Dispersion of S_0/A_0 ratio for composite plate.

4. FINITE ELEMENT SIMULATION

FE simulation of Lamb wave is carried out in three dimensions in aluminium and composite plates. Elements SOLID185 and SOLID226 are selected for modeling the aluminium and composite plates, as well as the PW patches respectively. Element SOLID185 is used for 3-D modeling of solid structures and is compatible for defining irregular regions. It is defined by eight nodes with three degrees of freedom at each one (i.e. translations in the nodal x, y, and z directions), while SOLID226 has 20 nodes with up to five degrees of freedom per node. ANSYS© is used here for FE simulation.

Selection of element size is crucial for FE simulation of wave propagation. The size of the elements must be sufficiently small for there to be at least 10 nodes per wavelength of the propagating wave.[15,16] Only A_0 and S_0 modes of Lamb wave are involved in the analysis and A0 mode has the smaller wavelength at 204 kHz which is 6.545 mm. Accordingly, the element size of 0.5 mm is used for the simulation.

The nodes on the upper and the lower faces of the PW transducer models are electrically coupled to form master nodes separately on both faces. Zero voltage constraint is applied to the master nodes at the bonded faces of the patches. Excitation voltage is applied to the master node on the top face in the case of the PW actuator and is measured at the master node on the same face from the PW sensor.

Newmark algorithm is used here for time integration in FE analysis with $\alpha = 0.25$ and $\delta = 0.5$, where α and δ are the Newmark parameters. For these values of α and δ, the Newmark algorithm is unconditionally stable. In this case, the time step size used is based on the trade-off between the desired accuracy and the computational efforts. The accuracy in the integrations can be stated in terms of period elongation and amplitude decay.[15,16]

In the FE simulation of Lamb wave propagation, both period elongation and amplitude decay affect the group velocity. Therefore, a convergence study is carried out as shown in Tables 1 and 2. This decides the appropriate mesh size and time step for a solution so the group velocities of A_0 and S_0 Lamb

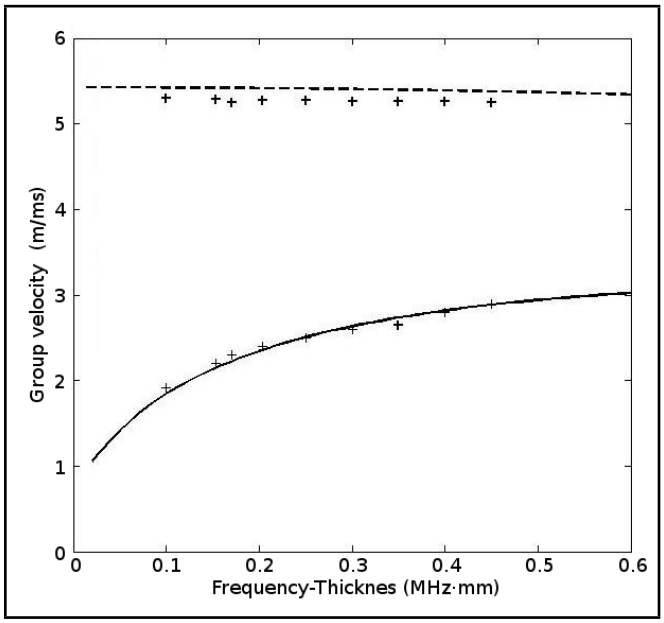

Figure 13. Comparison of analytical and FE simulation dispersion curves for an aluminium plate. The continuous line shows A_0 mode. The dotted line show S_0 mode, and $+$ shows FE simulation results.

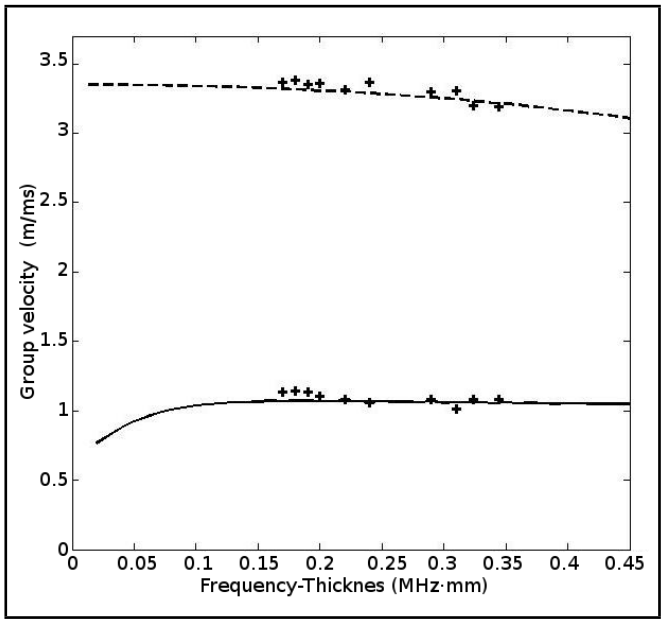

Figure 14. Comparison of analytical and FE simulation dispersion curves for an composite plate. Continuous line show A_0 mode and dotted line show S_0 mode, $+$ shows FE simulation results.

wave modes obtained through simulation are compatible with those obtained analytically, while requiring optimal simulation efforts in terms of simulation time and space required in the computer.

Accordingly, the time step 2×10^7 seconds is used for the simulation. With the above mentioned mesh size and time steps, the FE simulations are carried out for healthy state in frequencies ranging from 50 kHz to 350 kHz in the case of aluminium plates, and from 82 kHz to 170 kHz, in case of composite plates. Group velocities are then calculated. The comparison of group velocities through FE simulation is done with those obtained analytically and found to be in agreement, as shown in the Figs. 13 and 14. The 3-D FE simulations are carried out for 8.5 cycles, 10 volt, from peak to peak, Gaussian input signal having central frequencies of 204 kHz and 85 kHz, which are the 'sweet spot' frequencies,[12] as shown in Figs. 15 and 16. In this case, 12 responses are obtained for healthy and damaged plate each. Signal processing is carrried out for each response, which is discussed in the following section.

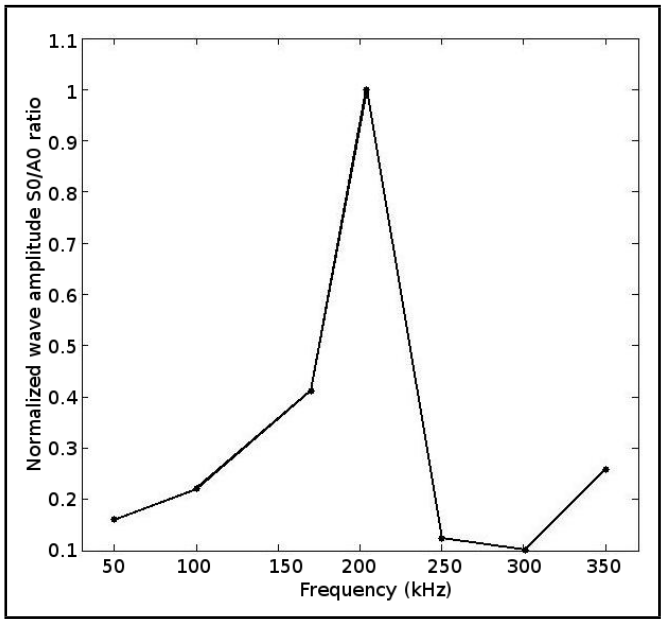

Figure 15. FE simulated dispersion of S_0/A_0 ratio for aluminium plate.

5. SIGNAL PROCESSING

Geodesic algorithm requires the arrival time for locating the damages. In the present work, continuous wavelet transform (CWT) is used to get the arrival times data and is discussed in the following subsection.

5.1. Continuous Wavelet Transform

According to Daubechies, CWT is defined as:[13]

$$C_f(a,b) = \frac{1}{\sqrt{a}} \int_{-\infty}^{\infty} f(t)\, \varphi * \left(\frac{t-b}{a}\right) dt; \qquad (8)$$

where, $f(t)$ is the input signal, a and b are real numbers called scale (or dilation) and position, respectively. $C_f(a,b)$ are the wavelet coefficients of the function $f(t)$, and $\phi\left(\frac{t-b}{a}\right)$ is the wavelet function, while the symbol $*$ denotes the complex conjugation.

A CWT allows the division of a continuous time function into wavelets from and the construction of a time-frequency representation of a given input signal. It is used here to obtain the arrival times. Fig. 17 shows the sample signal recorded for a pristine and a damaged plate for A_1S_2 (Actuator-1, Sensor-2) configuration at 204 kHz.

Wavelet transform is applied on the residual signal (the difference between damage and a healthy response) and obtained from the plot shown in Figs. 17 and 18. In the present study, the wavelet transform is carried out in a freeware AGU Vallen wavelet software.

Here, more emphasis is given on the residual signal, because it contains only the back-scattered reflection coming from the

Table 1. Selection of mesh size.

Mesh size (m)	Group velocity (m/s)				Simulation time (hrs.)	Memory (GB)
	S_0	Error with actual (%)	A_0	Error with actual (%)		
$0.1e^{-3}$	5035	8.653	2198.12	7.442	2:43	2.3
$0.2e^{-3}$	5167	6.259	2210.97	6.947	2:24	1.93
$0.3e^{-3}$	5207	5.533	2258.34	4.9263	2:09	1.81
$0.4e^{-3}$	5310	3.664	2285.17	3.789	1:45	1.55
$\mathbf{0.5e^{-3}}$	**4551**	**1.0319**	**2346.92**	**1.221**	**1:30**	**1.21**
$0.6e^{-3}$	5604	1.6817	2406.47	1.3052	1:10	1.04
$0.7e^{-3}$	5745	4.2271	2457.00	3.452	0:53	0.87

Table 2. Selection of time steps for Newmark integration.

Time step (μs)	Group velocity (m/s)				Simulation time (hrs.)	Memory (GB)
	S_0	Error with actual (%)	A_0	Error with actual (%)		
0.1	5425.93	1.561	2287.74	3.7052	02:24	1.93
0.2	**5465.56**	**0.8425**	**2336.16**	**1.6421**	**01:05**	**1.05**
0.3	5598.23	1.574	2418.71	1.8105	00:33	0.754
0.4	5627.13	2.0887	2455.52	2.9473	00:31	0.605
0.5	5713.7	6.6572	2481.81	4.4631	00:28	0.511

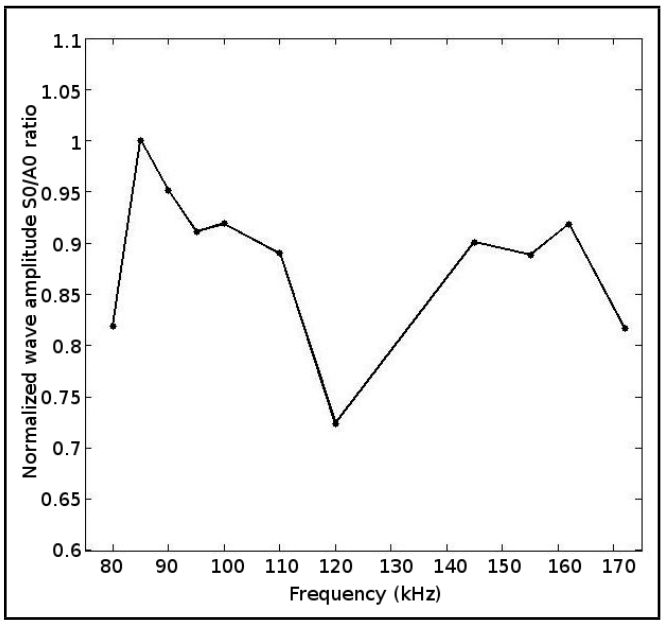

Figure 16. FE simulated dispersion of S_0/A_0 ratio for composite plate.

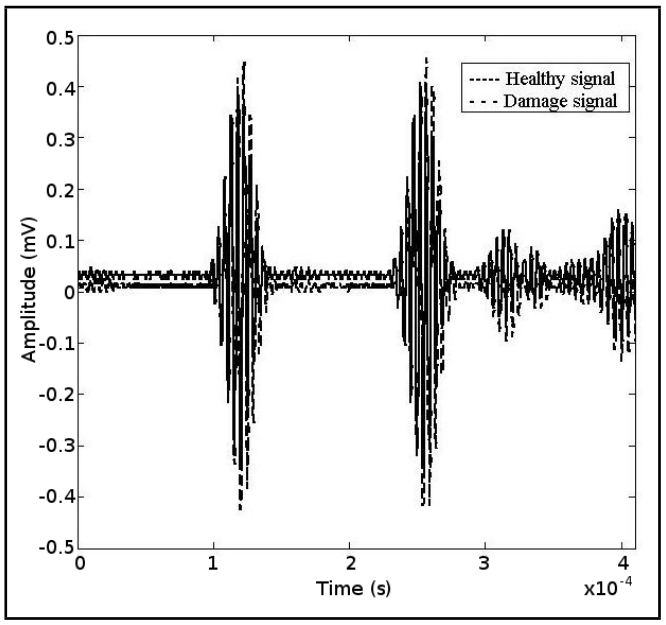

Figure 17. Experimental signal from a pristine and a damaged plate at 204 kHz.

damage, as well as from multiple scattering between the structural damage and the boundaries.[1]

Lamb wave is highly sensitive to the presence of any damages and its propagation is affected by irregularities, as revealed by peaks in Fig. 18. The arrival times are received pertaining to the peaks and are further used in the geodesic algorithm, which is discussed in the following subsection.

5.2. Geodesic Algorithm

The fundamental fact employed here is that a wave always takes minimum energy path to travel between any two points in the plate. For a homogeneous isotropic medium, this minimum path is the shortest distance also called the shortest geodesics.

On a plane, the geodesics are lines, while, on a sphere, the geodesics are circles. Once their paths are extracted in a given geometry, the defect location is reached by locating the intersections of the geodesics.[1] Consider two sensors, S_1 and S_2, located at (S_{1x} and S_{2x}), and (S_{1y} and S_{2y}) with V being the velocity of the wave in the medium. Let t_1 and t_2 be the time taken by the wave and generated from the damage S to reach the sensors, S_1 and S_2, respectively. The time taken to reach the two sensors is proportional to the distance between the source and the sensors. Therefore, the governing equation is given by:

$$D\left(S_1 - S\right) = Vt_1; \tag{9}$$

$$D\left(S_2 - S\right) = Vt_2; \tag{10}$$

If a source S is generated at a location at S_x and S_y in a planar surface then the distance between the source to sensor S_1 is given by:

$$D\left(S_1 - S\right) = \sqrt{\left(S_{1\mathrm{x}} - S_{\mathrm{x}}\right)^2 + \left(S_{1\mathrm{y}} - S_{\mathrm{y}}\right)^2}; \tag{11}$$

and the distance from the source to sensor S_2 is given by:

$$D\left(S_2 - S\right) = \sqrt{\left(S_{2\mathrm{x}} - S_{\mathrm{x}}\right)^2 + \left(S_{2\mathrm{y}} - S_{\mathrm{y}}\right)^2}. \tag{12}$$

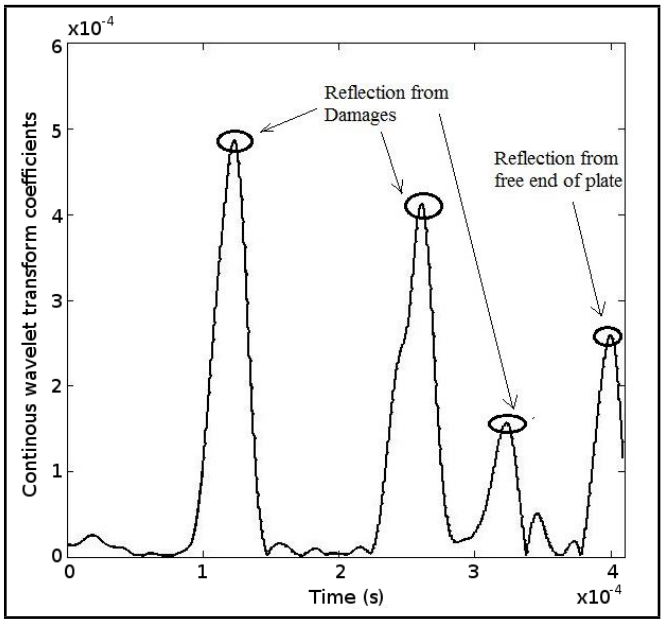

Figure 18. CWT coefficients computed at 204 kHz.

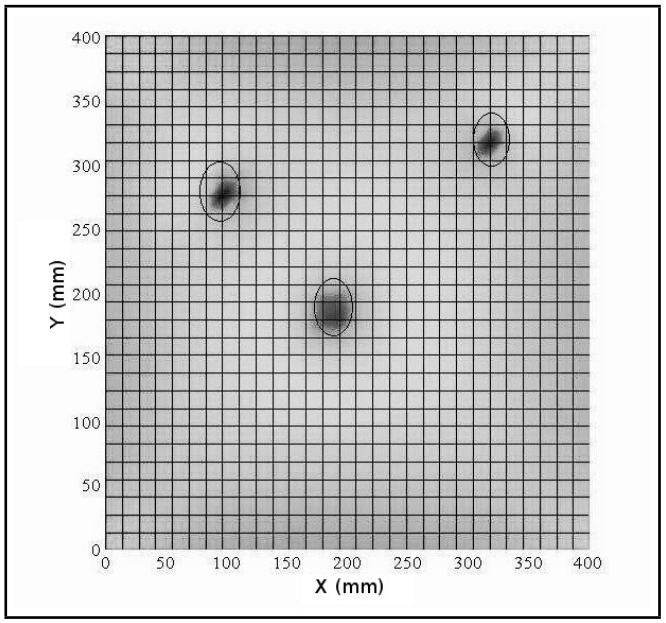

Figure 19. Experimentally located three damages by geodesic algorithm in an aluminium plate.

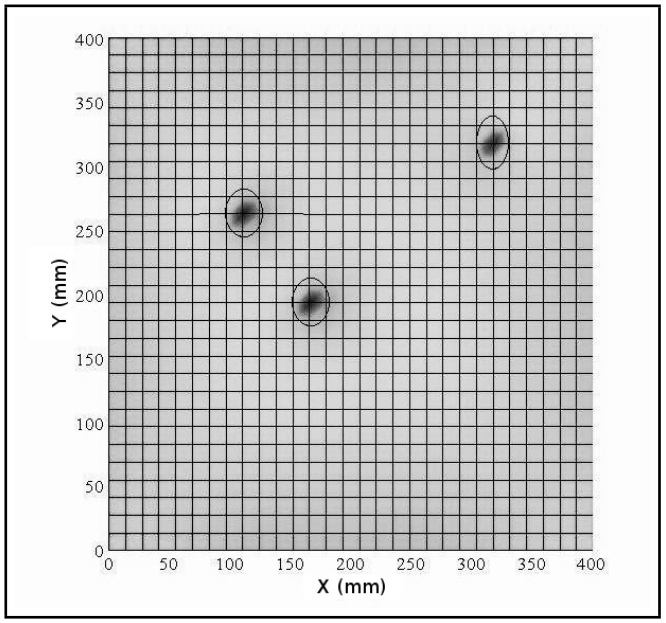

Figure 20. Experimentally located three damages by geodesic algorithm in a composite plate.

Once the geodesics from Eqs. (11) and (12) are obtained, the following step is to find intersections of only those geodesics which satisfy a particular condition. For a given mesh, let nk be the K^{th} node in the mesh and $D(nkS_i)$ be the distance between K^{th} node and i^{th} sensor. Geodesic distance between any sensors S_i and damage node is formed by nodes which satisfy the condition that:

$$D(nkS_i) = Vt_i; \tag{13}$$

where, t_i is the hit arrival time between the sensor S_i and damage and $D's$ are the geodesic distances and the corresponding curve can be seen as set of these nodes which is given by:

$$C_{ij} = nk|D(nkS_i) = Vt_i. \tag{14}$$

The intersection point or damage location in the set is given by:

$$S = (n|C1\text{s} \cap C2\text{s} \cap C3\text{s} \cap C4\text{s}). \tag{15}$$

A MATLAB© code is written for implementing Eqs. (9–15). Through it, the arrival times are used to obtain the damage locations. Damages are located at (185.6 mm, 183.4 mm), (319.4 mm, 319.2 mm), and (97.65 mm, 278.2 mm), in the case of an aluminium plate, shown in Fig. 19, and at (168.9 mm, 191 mm), (318.9 mm, 317.9 mm), and (105.1 mm, 254.5 mm), in the case of a composite plate, shown in Fig. 20, based on the experimentally obtained Lamb wave data.

Damages are located at (187.1 mm, 184.3 mm), (318.3 mm, 317.9 mm), and (96.4 mm, 279.4 mm) in the case of an aluminium plate, shown in Fig. 21, and at (169.1 mm, 189.6 mm), (317.5 mm, 318.6 mm), and (106.4 mm, 256.7 mm) in the case of a composite plate, shown in Fig. 22, based on the Lamb wave data from 3-D FE simulation. Both experimental and FE simulation techniques show close damage locations.

6. CONCLUSIONS

In this study, the interaction of A_0 Lamb wave mode with the multiple damages in an aluminium plate and a woven fiber composite laminate are examined. Lamb wave responses are obtained both experimentally and using 3-D FE simulation for a healthy plate at different frequencies, after which group velocities are calculated.

The group velocities are compared with those obtained analytically and found to be in agreement. This confirms effective actuation and sensing of Lamb wave in both plates.

Experimental and 3-D FE simulations are carried out on the healthy and the damaged aluminium and composite plates, and the Lamb wave responses are recorded. Arrival times of the wave from the damages using wavelet transform. Further, geodesic approach is used to locate three damages in both plates using the arrival time data. All three damages are located with a maximum error lying under 8 percent. Thus, the geodesic algorithm is shown to be effective in detecting multiple damages in both aluminium and composite plates.

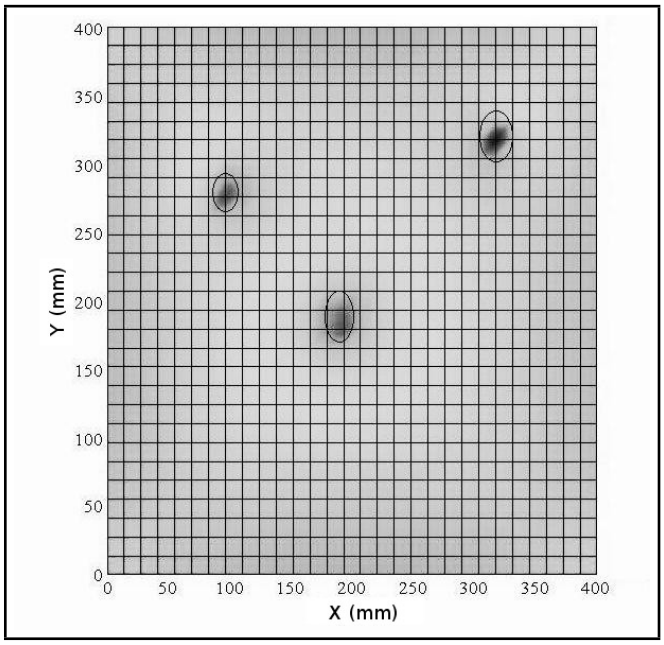

Figure 21. FE simulation located three damages by geodesic algorithm in an aluminium plate.

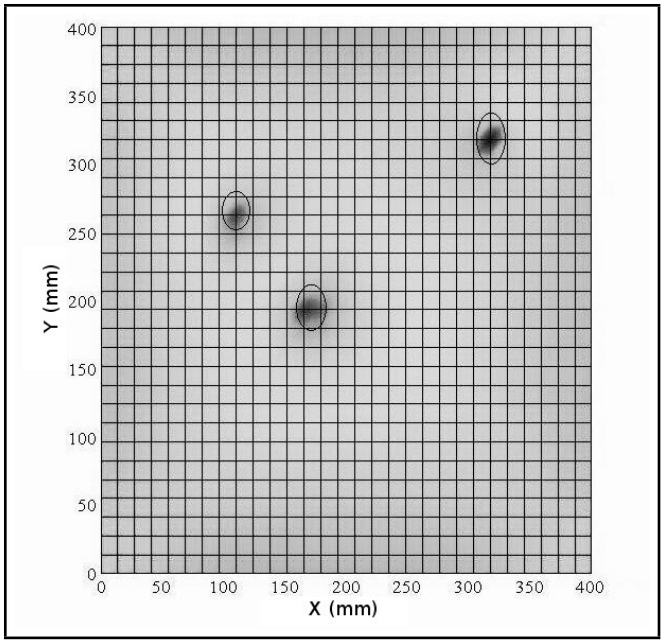

Figure 22. FE simulation located three damages by geodesic algorithm in a composite plate.

REFERENCES

[1] Gangadharan, R., Murthy, C. R. L., Gopalakrishnan, S., Bhat, M. R. and Mahapatra, D. R., Characterization of cracks and delaminations using PWAS AD Lamb wave based time-frequency methods, *International Journal on Smart Sensing and Intelligent Systems*, **3**(4), (2010).

[2] Raghavan, A. and Cesnik, C. E. S., Review of guided-wave structural health monitoring, *The Shock and Vibration Digest*, **39**(91), (2007).

[3] Zhongqing, S., Lin, Y. and Ye, L., Guided Lamb waves for identification of damage in composite structures: A review, *Journal of Sound and Vibration*, https://dx.doi.org/10.1016/j.jsv.2006.01.020, (2006).

[4] Beadle, B. M., Hurlebaus, S., Jacobs, L. J. and Gaul, L., Detection and localization of small notches in plates using Lamb waves, In *Proceedings of the 23rd International Modal Analysis Conference (IMAX XXIII)*, **96**, (2005).

[5] Mofakhami, M. R. and Boller, C., Scattering of Lamb waves from edge cracks in circular holes for understanding damage detection in more complex structures, *Materials forum*, **33**, (2009).

[6] Willberg, C., Perez, J. M., Ahmad, Z. and Gabbert, U., Simulation of piezoelectric induced Lamb wave in plates, *Proceedings in Applied Mathematics and Mechanics* **9**, (2009).

[7] Silva,C., Rocha, B. and Suleman, A., Guided Lamb waves based structural health monitoring through a PZT network system, *2nd International Symposium on NDT in Aerospace*, (2010).

[8] Kessler, S. S. and Spearing, S. M., Damage detection in composite materials using lamb wave methods, *Smart Materials and Structures* **11**, 269–278 (2002)

[9] Yamada, H., Mizutani, Y., Nishino, H., Takemoto, M. and Ono, K., Lamb wave source location of impact on anisotropic plates, *Proceedings of EW-GAE 2000 European Working Group on Acoustic Emission*, 77–83 (2000).

[10] Li, J. and Liu, S., The application of time-frequency transform in mode identification of Lamb waves, *17th World Conference on Non-destructive Testing*, **25**(28), (2008).

[11] Zabel, V. and Brehm, M., Wavelet analysis in structural health monitoring and damage detection, *Proceedings of the SAMCO Summer Academy*, **5**(9), (2005).

[12] Giurgiutiu, V., Bao, J. and Zhao, W., Piezoelectric wafer active sensor embedded ultrasonics in beams and plates, *Society for Experimental Mechanics*, **43**(4), 428–449 (2003).

[13] Liu, X., Leimbach, K. R., Hartmann, D. and Hoffer, R., Signal analysis using wavelets for structural damage detection applied to wind energy converters, *14th International conference on computing in civil and building engineering*, **27**(79), (2012).

[14] Baid, H. K., *Detection of Damage in a Composite Structure Using Guided Waves*, Ph. D. thesis, University of California, Los Angeles.

[15] Yelve, N. P., Mitra, M. and Mujumdar, P. M., Spectral damage index for estimation of breathing crack depth in an aluminum plate using nonlinear Lamb wave, *Structural Control and Health Monitoring*, https://dx.doi.org/10.1002/stc.1604, (2013).

[16] Yelve, N. P., Mitra, M. and Mujumdar, P. M., Higher harmonics induced in Lamb wave due to partial debonding of piezoelectric wafer transducers, *NDT&E International*, **63**, 21–27 (2014).